Powder snow avalanches: Approximation as non-Boussinesq clouds with a Richardson number–dependent entrainment function

C. Ancey

Environmental Hydraulics Laboratory, Swiss Federal Institute of Technology, Lausanne, Switzerland

Received 14 May 2003; revised 10 November 2003; accepted 28 November 2003; published 27 January 2004.

[1] This paper presents an investigation into non-Boussinesq particle-driven gravity currents such as powder snow avalanches and pyroclastic flows. For a finite-volume current to maintain its non-Boussinesq character (i.e., a substantial density difference with its surroundings) and therefore high velocities, it must counterbalance the entrainment of surrounding fluid by entraining particles from the bed. A number of theoretical models have assumed that the volume growth rate of such currents is controlled by the local slope and the density ratio between the current and the ambient fluid. An alternative assumption, according to which the volume growth rate is controlled solely by the overall Richardson number, is examined here. Both assumptions were used successively in the same theoretical model, primarily developed by A. G. Kulikovskiy and E. I. Sveshnikova, then by P. Beghin. The model predictions were compared to laboratory experiments (release of a finite volume down an inclined channel, with particle entrainment from the bed) and field data (a well-documented large powder snow avalanche in Switzerland). In both cases, the assumption of a slope-dependent volume growth rate received little support, whereas assuming that the entrainment coefficient is controlled by the Richardson number makes it possible to describe the velocity and volume variations fairly well, except for highly concentrated particle-driven currents in the laboratory. *INDEX TERMS:* 1815 Hydrology: Erosion and sedimentation; 1863 Hydrology: Snow and ice (1827); 4568 Oceanography: Physical: Turbulence, diffusion, and mixing processes; *KEYWORDS:* entrainment, Boussinesq approximation, snow, avalanche, Richardson number

Citation: Ancey, C. (2004), Powder snow avalanches: Approximation as non-Boussinesq clouds with a Richardson number–dependent entrainment function, *J. Geophys. Res.*, *109*, F01005, doi:10.1029/2003JF000052.

1. Introduction

[2] Particle-driven gravity currents are frequently encountered in nature [*Simpson*, 1997]. Typical examples include powder snow avalanches, pyroclastic flows down volcano slopes, and turbidity currents in the ocean. These currents take the form of a cloud or a stream of solid particles maintained in suspension by turbulence in the carrier fluid. Motion is produced by the density contrast between the suspension and the surrounding fluid. Since the surrounding fluid is entrained into the current, the solid concentration decreases inside the current, leading, in turn, to a decrease in the buoyancy force unless the current is supplied by a sufficiently strong input of particles. When the density difference between the current and the surrounding fluid is sufficiently small, the Boussinesq approximation, which neglects density differences except in buoyancy terms, is often used to simplify the equations of motion and the analysis of the behavior. Basically, this approximation does not hold for solid particles in the air as soon as the solid concentration exceeds a few percent; the flow is then said to be in a non-Boussinesq regime.

[3] The objective of this paper is to investigate the behavior of a particle cloud in a non-Boussinesq regime along an inclined surface. For this purpose a simplified theoretical model, hereinafter referred to as the Kulikovskiy-Sveshnikova-Beghin (KSB) model, will be introduced. In addition to the driving force (buoyancy), this model takes into account two competing processes: bed erosion and entrainment of the surrounding fluid into the cloud. Indeed, for the cloud to maintain its non-Boussinesq character an entrainment of particles from the bed is needed to offset cloud diffusion from fluid entrainment at the current interface. Different assumptions can be made concerning the entrainment rate. This paper will provide evidence that expressing the entrainment rate as a function of the Richardson number yields consistent results.

[4] The paper begins by reviewing the literature devoted to modeling particle clouds, which is very closely related to modeling powder snow avalanches. Then, the equations of motion used in the KSB model will be presented. A key problem is the definition of the volume growth rate. The first of two assumptions to be used here, suggested by *Kulikovskiy and Sveshnikova* [1977] and consistent with

0148-0227/04/2003JF000052$09.00

similarity solutions obtained for plumes, is to express the cloud growth rate as a function of the square root of the density ratio between the cloud and the ambient fluid. *Beghin* [1979] supplemented this assumption by introducing a dependence on the bed slope. This second assumption, consistent with the interpretation proposed by *Ellison and Turner* [1959] for inclined plumes, states that the growth rate is controlled solely by the overall Richardson number. Both assumptions will be tested against (unpublished) experimental data obtained by *Beghin* [1979] in the laboratory with an inclined closed channel. Finally, the KSB model predictions will be compared to field data recorded by the Swiss Federal Institute of Snow and Avalanche Research in La Sionne valley [*Dufour et al.*, 2001].

2. Previous Research

[5] Except for the recent developments on non-Boussinesq plumes [*Rooney and Linden*, 1996; *Woods*, 1997], the study of non-Boussinesq currents has long been tightly linked to the modeling of powder snow avalanches. Here, the term powder snow avalanche refers to an avalanche flowing in the form of a cloud of ice particles maintained in suspension by turbulence [*McClung and Schaerer*, 1993; *Ancey*, 2001]. Typically, flow depth, mean velocity, and mean density are of order 10–100 m, 40–100 m s^{-1}, and 1–25 kg m^{-3}, respectively. A great deal of research has been done to develop theoretical and numerical models of this flow (for an overview, see *Hutter* [1996]).

[6] The first-generation models used the analogy of density currents along inclined surfaces. Extending *Ellison and Turner*'s [1959] model on the motion of an inclined plume, *Hopfinger and Tochon-Danguy* [1977] modeled the mean velocity of a steady current, assumed to represent the avalanche body behind the head. They found that the front velocity of the current was only weakly dependent on the bed slope. Their results were supplemented by *Britter and Linden* [1980], who showed that bed slope has a significant effect on the entrainment of the surrounding fluid into the current and, thus, the current shape. For gentle slopes the current took the form of a head slightly deeper than the following tail, while for mild and steep slopes it looked like a semielliptic cloud. Their results can be explained as follows: Since the bottom drag is not sufficient to counterbalance the driving gravity force, the only way for a current to reach a steady state is to entrain the surrounding fluid and reduce the buoyant density. Further important theoretical contributions to modeling steady density currents were provided by *Parker et al.* [1986], *Stacey and Bowen* [1988], *Baines* [2001], and others. Notably, *Parker et al.* [1986] developed complete depth-averaged equations of motion including mass, momentum, and turbulent kinetic energy balance equations. It is, however, unclear how these results obtained for fairly steady density currents can be applied to real powder snow avalanches since the latter are closer to finite-length, unsteady currents than to constant supply flows.

[7] The second generation of models has considered the avalanche as a finite-volume turbulent flow of a snow suspension. *Kulikovskiy and Sveshnikova* [1977] presented a theoretical model (the KS model), in which the cloud was defined as a semielliptic body, whose volume varied with time [see also *Eglit and Revol*, 1998; *Bozhinskiy and Losev*, 1998]. The kinematics are entirely described by the mass center position and two geometric parameters of the cloud (the two semiaxes of the ellipse). The cloud density can vary depending on air and snow entrainment. *Kulikovskiy and Sveshnikova* [1977] obtained a set of four equations describing the mass, volume, momentum, and Lagrangian kinetic energy balances. The idea was subsequently redeveloped by *Beghin* [1979], *Beghin et al.* [1981], *Beghin and Brugnot* [1983], *Fukushima and Parker* [1990], *Beghin and Olagne* [1991], *Akiyama and Ura* [1999], *Fukushima et al.* [2000], etc. In its primary formulation, Beghin's model focused on two-dimensional Boussinesq clouds and ignored particle entrainment, sedimentation, and basal friction. The chief difference between the KS model and Beghin's model is that Kulikovskiy and Sveshnikova included a fourth equation (a Lagrangian kinetic balance equation), whereas energy aspects were ignored in Beghin's treatment. Extensions to Beghin's model were then added to account for the influence of bottom drag, three-dimensional spreading, etc. When compared to field data, this model has been found to provide a correct estimate of the front velocity, but the predicted cloud dimensions are in poor agreement with the data [*Nishimura et al.*, 1995; *Ancey*, 2004].

[8] The basic assumption underlying each model class (finite-volume/constant supply flow of a homogeneous turbulent suspension) is a rather stringent condition that is poorly supported by field observations. A new generation of powder snow avalanche models has recently appeared [*Hutter*, 1996]. Some rely on the numerical resolution of local equations of motion, including a two-phase mixture approximation and closure equations (usually a $k-\varepsilon$ model for turbulence) [*Scheiwiller et al.*, 1987; *Sampl*, 1993; *Naaim and Gurer*, 1997]. Other researchers have tried to establish a relation between a dense core and an airborne avalanche based on the premise that the core must supply snow to the airborne avalanche [*Eglit*, 1983, 1984, 1998; *Nazarov*, 1991; *Issler*, 1998]. Though these recent developments are undoubtedly a promising approach to modeling powder snow avalanches, their level of sophistication contrasts with the crudeness of their basic assumptions as regards the momentum exchanges between phases and turbulence modification due to the dispersed phase, interactions with snow cover, density stratification, and changes in the snow features (snowball size, water content). At this level of our knowledge of physical and natural processes it is of great interest to continue to use simple models and to fully explore what they can describe and explain.

[9] This paper presents a simple model, directly inspired from Beghin's model and the KS model: We will refer to it as the Kulikovskiy-Sveshnikova-Beghin (KSB) model. Here, we take advantage of the growing knowledge of density and turbidity currents and of entrainment mechanisms as well as the information gathered from the catastrophic winters of 1981 and 1999 in the Alps [*Ammann*, 2000]. Compared to the KS model, this extended model better accounts for the influence of particle current mixing with the ambient fluid. In addition, the KSB model applies equally to Boussinesq and non-Boussinesq flows. The KSB model aims at describing the motion of powder snow avalanches in their flow phase, but it is not intended to

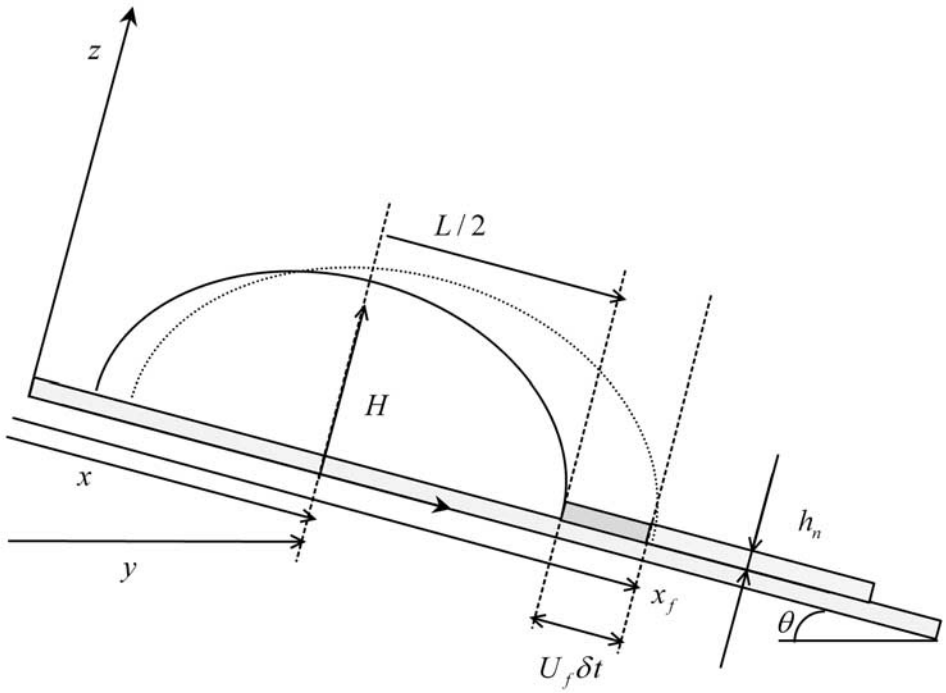

Figure 1. Sketch of the physical system studied here.

describe the run-out phase, for which additional processes (turbulence, particle sedimentation, bottom drag, etc.) must be taken into account. The KSB model should also apply to other density surges such as pyroclastic currents and turbidity currents in the ocean.

3. KSB Model

[10] In the following we will consider the two-dimensional motion of a cloud along a curvilinear profile. The profile can be described by a smooth and gently varying curve in the form $z = f(y)$, where z is the elevation and y is an arbitrary distance measured along a horizontal axis. The mass center of the cloud has the curvilinear abscissa x given by $x = \int_0^y \sqrt{1 + f'^2(y)}dy$ taken from an arbitrary point of origin. If the radius of curvature $((1 + f'^2(y))^{3/2}/f''(y))$ is large relative to the typical length of the cloud L, then everything happens locally, as if the path were an infinite plane inclined at an angle $\tan\theta(y) = f'(y)$ with respect to the horizontal.

[11] Figure 1 depicts a typical cloud entraining particles from the bed. In the following, H denotes the cloud height, L length, m mass, and V volume. The cloud velocity is $U = d\,x/dt$ but, since the body is deformable, the velocity varies inside the body. The front position is given by the abscissa x_f and its velocity is $U_f = dx_f/dt$. The volume solid concentration is φ, and it is assumed that the cloud is a homogeneous suspension of particles of density ρ_p (no density stratification) in the ambient fluid of density ρ_a and viscosity μ_a. The bulk cloud density is then $\bar{\rho} = \varphi\ \rho_p + (1 - \varphi)\rho_a$. Ahead of the front, there is a particle bed of thickness h_n, which is made up of the same particles as the cloud. The apparent density of the layer is $\rho_s = \varphi_m\rho_p + (1 - \varphi_m)\rho_a$, where φ_m denotes the maximum random volume concentration of particles.

[12] The surface area (per unit width) exposed to the surrounding fluid is denoted S and can be related to H and L as follows: $S = k_s\sqrt{HL}$, where k_s is a shape factor. Here we assume that the cloud keeps a semielliptic form, whose aspect ratio $k = H/L$ remains constant when the slope is constant. We then obtain

$$k_s = \mathrm{E}\left(1 - 4k^2\right)/\sqrt{k}, \tag{1}$$

where E denotes the elliptic integral function. Similarly, we can also express the volume V (per unit width) as $V = k_v HL$, where k_v is another shape factor for a half ellipsis. Here we have

$$k_v = \pi/4. \tag{2}$$

In the following we will also need to use the volume, height, and length growth rates:

$$\alpha_v = \frac{1}{\sqrt{V}}\frac{dV}{dx}, \alpha_h = \frac{dH}{dx}, \alpha_l = \frac{dL}{dx}. \tag{3}$$

Experimentally, it is easier to measure the growth rates using the cloud front, rather than its center of mass; we will refer to these rates as

$$\tilde{\alpha}_v = \frac{1}{\sqrt{V}}\frac{dV}{dx_f}, \tilde{\alpha}_h = \frac{dH}{dx_f}, \tilde{\alpha}_l = \frac{dL}{dx_f}. \tag{4}$$

Note that all these quantities are interrelated. For instance, using $x = x_f - L/2$, we find $\tilde{\alpha}_h = (dH/dx)(dx/dx_f) = \alpha_h(1 -$

$\tilde{\alpha}_l/2$). Similarly, using the definition of k and k_v, we obtain

$$\alpha_h = \frac{\alpha_v}{2}\sqrt{\frac{k}{kv}} \text{ and } \alpha_l = \frac{\alpha_v}{2\sqrt{kkv}}. \quad (5)$$

The KSB model includes three equations: volume, mass, and momentum balances. Compared to the highly developed model proposed by *Fukushima and Parker* [1990], we do not take into account the turbulent kinetic energy equation. On the one hand, in their numerical simulation, *Fukushima and Parker* [1990] found that this equation plays a role mostly in the run-out phase. On the other hand, an equation of this type involves a number of additional parameters that are difficult to determine, and thus in the present framework, where the simplest model is sought, it is interesting to test whether it is possible to obtain good predictions without using this equation.

3.1. Volume Equation

[13] Changes in cloud volume result primarily from the entrainment of the ambient, less dense fluid. Various mixing processes are responsible for the entrainment of the ambient fluid into the cloud. It has been shown for jets, plumes, and currents that (1) different shear instabilities (Kelvin-Helmoltz, Hölmböe, etc.) can occur at the interface between dense and less dense fluids and that (2) the rate of growth of these instabilities is controlled by a Richardson number [*Turner*, 1986; *Fernando*, 1991; *Strang and Fernando*, 2001], defined here:

$$\mathrm{Ri} = \frac{g' H \cos\theta}{U^2}, \quad (6)$$

where g' denotes the reduced gravity $g' = g\Delta\bar{\rho}/\rho_a$ and $\Delta\bar{\rho} = \bar{\rho} - \rho_a$ is the buoyant density.

[14] Note that the Richardson number is the inverse square of the Froude number used in hydraulics. The Richardson number can be seen as the ratio of the potential energy ($g\Delta\bar{\rho}H\cos\theta$) to the kinetic energy ($\rho_a U^2$) of a parcel of fluid at the current interface. Usually a smaller Ri implies predominance of inertia effects over the restoring action of gravity and thus greater instability and a higher entrainment rate; it is then expected that the entrainment rate is a decreasing function of the Richardson number. Mixing is observed to occur in gravity currents due to the formation of Kelvin-Helmoltz (K-H) billows at the front, which grow in size, are advected upward, and finally collapse behind the head; the lobe-and-cleft instability is also an efficient mechanism of entrainment [*Simpson*, 1972, 1997].

[15] Although the details of the mixing mechanisms are very complex, a striking result of recent research is that their overall effects can be described quite simply [*Turner*, 1973, 1986; *Fernando*, 1991]. In terms of the cloud volume balance, the commonest assumption is to state that the volume variations come from the entrainment of the ambient fluid into the cloud and that the inflow rate is proportional to the exposed surface area and a characteristic velocity u_e. This leads to the equation

$$\frac{dV}{dt} = E_v S u_e, \quad (7)$$

where E_v is the bulk entrainment coefficient. According to the flow conditions, different expressions of E_v have been drawn from experiments. Interestingly, the value of E_v has been expressed very differently, depending on whether the current is steady or unsteady. In the following we examine these expressions in the case of steady currents (section 3.1.1) and unsteady currents or clouds (section 3.1.2). There is, however, no clear physical reason justifying this partitioning. Indeed, for most experiments the currents were gradually accelerating, and mixing still occurred as a result of the development of K-H billows [*Pawlack and Armi*, 1998], as in the steady case. This prompts us to propose a new expression of the entrainment coefficient for clouds (section 3.1.3), which holds for both steady and slightly unsteady conditions.

3.1.1. Entrainment Assumption for Steady Jets and Currents

[16] For jets and plumes the similarity solutions to the equations of motion lead to selecting $u_e = U$ (U is the depth-averaged velocity) for Boussinesq flows [*Turner*, 1973] and $u_e = \sqrt{\bar{\rho}/\rho_a}U$ for non-Boussinesq flows [*Rooney and Linden*, 1996], in agreement with experimental data. In both cases, E_v is a constant close to 0.13 [*Linden*, 2000].

[17] The behavior of inclined plumes is not as well understood and somewhat controversial [*Turner*, 1986]. For constant supply inclined plumes, it has been found that E_v is not a constant but depends on the dimensionless numbers involved in the problem, including the overall Richardson number, the bed slope θ, and, to a lesser extent, the flow Reynolds number. Experimental investigations have shown that the Ri dependence of the E_v can be expressed as

$$E_v = H'(x) \approx a\mathrm{Ri}^{-n}, \quad (8)$$

where $a(\theta)$ and n are parameters. For steady inclined plumes, *Turner* [1986] provided the relationship $E_v = (0.08-0.1\mathrm{Ri})/(1 + 5\mathrm{Ri})$, implying $E_v = 0$ for $\mathrm{Ri} > 0.8$, whereas *Baines* [2001] found for $\theta = 0$ and for $0.1 < \mathrm{Ri} < 10$ that $a = 0.001$ and $n = 1$. Surprisingly, the more detailed investigation on sheared density interface conducted by *Strang and Fernando* [2001] gave very different values (a factor of 10 higher): $E_v \to 0.024$ for $\mathrm{Ri} \to 0$, $a = 0.22 \pm 0.11$ and $n = 2.63 \pm 0.45$ for $1.5 < \mathrm{Ri} < 5$ (K-H instabilities are the prevailing mixing agent), and $a = 0.02 \pm 0.01$ and $n = 1.3 \pm 0.15$ for $5 < \mathrm{Ri}$.

[18] As advocated by *Ellison and Turner* [1959], for a steady current down a plane inclined at an angle θ, there must be a Richardson number, called the normal Richardson number (in analogy with the normal depth reached by a gradually varied flow of water in an open-channel flow), toward which the overall Richardson number adjusts. If the flow decelerates (lower U value), the Richardson number increases, leading to a decrease in the inflow rate and the conservation of the buoyant density; gravity then accelerates the flow. On the other hand, if the flow accelerates, the Richardson number drops, allowing the current to entrain more ambient fluid and dilute. Furthermore, *Ellison and Turner* [1959] showed that the normal Richardson number Ri_n is a function of the bed slope θ. It follows that for fully developed currents the entrainment coefficient $E_v(\theta, \mathrm{Ri})$ comes close to $E_v(\theta, \mathrm{Ri}_n)$ and becomes only a function of

the slope $E_v(\theta)$, which implies that it is experimentally difficult to discriminate the dependence of E_v on θ and Ri.

3.1.2. Entrainment Assumption for Unsteady Currents and Clouds

[19] For unsteady currents and clouds with a constant volume of particles (thermals), a number of experiments have been done to measure the entrainment coefficient. For the head preceding a steady inclined current, *Britter and Linden* [1980] expressed the growth rates of the cloud height and length as a function only of the bed slope, implying that the coefficient of entrainment E_v also depends on the slope. For a cloud with a constant volume of particles, *Beghin* [1979] also found a linear growth rate controlled by the slope $\tilde{\alpha}_h = dH/dx_f = 0.0036\theta + 0.04$ (θ expressed in degrees) and $\tilde{\alpha}_l = dL/dx_f = 0.0044\theta + 0.26$ for Boussinesq clouds, giving a volume growth rate $\alpha_v = k_s E_v/\sqrt{k_v} = 2\sqrt{k_v}\tilde{\alpha}_h/\left(\sqrt{k}(1-\tilde{\alpha}_l/2)\right)$, i.e., a function of the slope that we will denote $\alpha(\theta)$ in the following.

[20] For non-Boussinesq clouds, Beghin observed a departure from linear growth, which he ascribed to the large density difference between the cloud and the surrounding fluid. Following *Kulikovskiy and Sveshnikova* [1977], he suggested that for a non-Boussinesq cloud the height increase should be affected by a coefficient $\sqrt{\rho(a)/\bar{\rho}}$: $H \propto \sqrt{\rho_a/\bar{\rho}}\ \alpha_h(\theta)\ x$.

[21] Note that this form is consistent with an entrainment velocity in the form $u_e = \sqrt{\bar{\rho}/\rho_a}U$ (this can be shown by considering the mass equation $d\ (\bar{\rho}V)/dt = \rho_a dV/dt = \rho_a E_v S u_e$). Although the few experimental results performed by Beghin were qualitatively consistent with this formulation of the entrainment rate, there is no clear evidence from a quantitative viewpoint that Beghin's statement is correct.

3.1.3. A New Entrainment Assumption for Clouds

[22] A very different interpretation of Beghin's data can be proposed. As shown experimentally and supported theoretically [*Beghin*, 1979; *Beghin et al.*, 1981], the overall Richardson number of a Boussinesq cloud quickly tends toward a slope-dependent value since $U \propto 1/\sqrt{x}$, $H \propto x$, and $\Delta\bar{\rho} \propto 1/x^2$. The situation is close to that occurring for steady inclined plumes, in that $\mathrm{Ri} \to \mathrm{Ri}_n(\theta) = (3/2)\alpha_h(1+\chi)\tan^{-1}\theta$. This makes it possible to relate the cloud growth rate E_v (or α_v) to the overall Richardson number.

[23] Figure 2 shows how $\tilde{\alpha}_h$ and α_v vary with Ri for a Boussinesq cloud (data from *Beghin et al.* [1981]). It can be seen that, as expected, $\tilde{\alpha}_h$ is a decreasing function of the Richardson number. A rational expression structurally close to that proposed by *Turner* [197]] has been fitted:

$$\tilde{\alpha}_h = \frac{1.53 - \mathrm{Ri}}{4.1 + 2.96\mathrm{Ri}}. \tag{9}$$

It is then possible to relate E_v (or α_v) as a function of Ri instead of θ. Obviously, there is little difference between the two formulations in the case of Boussinesq clouds, but for non-Boussinesq clouds, they lead to very different behaviors immediately following avalanche release: Insofar as the density difference $\bar{\rho}$ is great and the cloud velocity is close to zero, the Richardson number is very large: $\mathrm{Ri} \gg 1$. If the entrainment rate is given by $E_v(\mathrm{Ri})U$, this means that the surrounding fluid entrainment is very low, whereas if the entrainment rate is $\alpha(\theta)\sqrt{\bar{\rho}/\rho_a}U$, there is a substantial increase in cloud volume. Since there is no clear experimental evidence supporting one or the other formulation, we will test both in the next section.

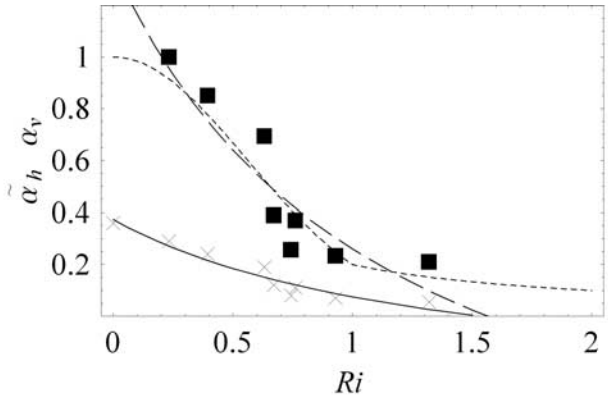

Figure 2. Variation in the growth rates of the cloud height $\tilde{\alpha}_h$ (crosses) and volume α_v (solid squares) with the overall Richardson number. Data are from *Beghin et al.* [1981]; the Richardson number was evaluated by using the relationship $Ri_n(\theta) = (3/2)\alpha_h(1+\chi)\tan^{-1}\theta$, where α_h is the value given in Table 1 of *Beghin et al.* [1981]. The solid line represents the rational function $\tilde{\alpha}_h = (1.53 - \mathrm{Ri})/(4.1 + 2.96\ \mathrm{Ri})$ fitted on the *Beghin et al.* [1981] data using the least squares method. The long-dashed line stands for the rational function $\alpha_v = (1.56 - \mathrm{Ri})/(1.16 + 1.01\ \mathrm{Ri})$ fitted to the experimental values of the volume growth rate, while the dashed line represents the two-piece function: if $\mathrm{Ri} \le 1$, then $\alpha_v = e^{-1.6}\mathrm{Ri}^2$, and for $\mathrm{Ri} > 1$, $\alpha_v = 0.2/\mathrm{Ri}$.

3.1.4. Summary

[24] From this discussion of the entrainment assumption we retain the following equation for the volume variations:

$$\frac{dV}{dt} = \alpha_v\sqrt{V}U, \tag{10}$$

where (1) if the bulk entrainment coefficient E_v is assumed to be a function of the overall Richardson number, then $\alpha_v = E_v(\mathrm{Ri})\ k_s/\sqrt{k_v}$, and (2) if E_v is slope-dependent, $\alpha_v = \sqrt{\bar{\rho}/\rho_a}E_v(\theta)k_s/\sqrt{k_v}$.

3.2. Mass Balance Equation

[25] The cloud mass can vary as a result of the entrainment of the surrounding fluid and/or the entrainment of particles from the bed. The former process is easily accounted for: During a short time increment δt, the cloud volume V is increased by a quantity δV mainly as a result of the air entrainment; thus the corresponding increase in the cloud mass is $\rho_a \delta V$. The latter process is less well known. In close analogy with sediment erosion in rivers and turbidity currents, *Fukushima and Parker* [1990] assumed that particles are continuously entrained from the bed when the drag force exerted by the cloud on the bed exceeds a critical value. This implies that the particle entrainment rate depends on the surface of the bed in contact with the cloud and that the drag force is in excess of the threshold of motion. However, the recent experiments by *Capart and Young* [1998] and the numerical simulations by *Fraccarollo and Capart* [2002] together

with *Pritchard and Hogg*'s [2002] theoretical model have shown that for a suddenly released fluid (a dam break problem), entrainment of particles occurs mainly in the flow snout. In this case the entrainment rate is controlled solely by the front features.

[26] In extreme conditions the upper layers of the snow cover are composed of new snow of weak cohesion and can be easily entrained. Thus it is reasonable to think that all the recent layer ahead of the cloud is incorporated into the cloud: When the front has traveled a distance $U_f\delta t$, where U_f is the front velocity, the top layer of depth h_n and density ρ_s is entirely entrained into the cloud (see Figure 1). The resulting mass variation (per unit width) is $\rho_s U_f h_n \delta t$. At the same time, particles settle with a velocity v_s. During the time step δt, all the particles contained in the volume $Lv_s\delta t$ deposit. Finally, by taking the limit $\delta t \to 0$, we can express the mass balance equation as follows:

$$\frac{dm}{dt} = \rho_a \frac{dV}{dt} + \rho_s U_f h_n - \varphi \rho_s L v_s,$$

where $m = \bar{\rho}V$ is the cloud mass. Usually, the settling velocity v_s is very small compared to the mean forward velocity of the front such that it is possible to ignore the third term in the right-hand side of the equation above. We then obtain the following simplified equation:

$$\frac{d\Delta\bar{\rho}V}{dt} = \rho_s U_f h_n. \tag{11}$$

3.3. Momentum Balance Equation

[27] The cloud undergoes the driving action of gravity and the resisting forces due to the ambient fluid and the bottom drag. The driving force per unit volume is $\bar{\rho}g \sin\theta$. Usually, the bottom frictional force is written in a Chézy form: $C_D\bar{\rho}U^2L$, where $C_D(\mathrm{Re})$ is the Chézy friction factor, dependent on the overall Reynolds number. Bottom drag typically plays a minor role in the accelerating and steady flow phases but becomes significant in the decelerating phase [*Hogg and Woods*, 2001]. Since we have set aside a number of additional effects (particle sedimentation, turbulent kinetic energy), it seems reasonable to also discard this frictional force. The action of the ambient fluid can be broken into two terms: a term analogous to a static pressure (Archimedes's theorem), equal to $\rho_a Vg$, and a dynamic pressure. As a first approximation, the latter term can be evaluated by considering the ambient fluid as an inviscid fluid in an irrotational flow. On the basis of this approximation, it can be shown that the force exerted by the surrounding fluid on the half cylinder is $\rho_a V\chi dU/dt$, where

$$\chi = k \tag{12}$$

is called the added mass coefficient [*Batchelor*, 1967]. Since at the same time volume V varies and the relative motion of the half cylinder is parallel to its axis of symmetry, we finally take $\rho_a\chi d\,(UV)/dt$ [*Lhuillier*, 1982]. Note that this parameter could be ignored for light interstitial fluids (e.g., air), whereas it has a significant influence for heavy interstitial fluids (basically, water). Thus the momentum balance equation can be written as

$$\frac{d(\bar{\rho} + \chi\rho_a)VU}{dt} = \Delta\bar{\rho}gV \sin\theta. \tag{13}$$

3.4. Asymptotic and Approximate Solutions

[28] We consider the motion of a cloud along a plane inclined at an angle θ to the horizontal. Analytical solutions can be found for equations (10), (11), and (13) in the case of a Boussinesq flow ($\bar{\rho}/\rho_a \to 1$) (see Appendix A); for the other cases, numerical methods must be used. In the Boussinesq limit, since the final analytical solution is complicated (see Appendix A), we only provide an asymptotic expression at early and late times. To simplify the analytical expressions, without loss of generality, we take $U_0 = 0$ and $x_0 = 0$, and we assume that the erodible snow cover thickness h_n and density ρ_s are constant. The other initial conditions are at $t = 0$ and $x = 0$, $H = H_0$, $L = L_0$, $V_0 = k_v H_0 L_0$, and $\bar{\rho} = \bar{\rho}_0$. At short times the velocity is independent of the entrainment parameters and the initial conditions ($\bar{\rho}_0$ and V_0):

$$U \propto \sqrt{2gx\sin\theta \frac{\Delta\rho_0}{\Delta\rho_0 + (1+\chi)\rho_a}} \approx \sqrt{2gx\sin\theta}, \tag{14}$$

where we used $\rho_a \ll \Delta\bar{\rho}_0$. This implies that the cloud accelerates vigorously in the first instants ($dU/dx \to \infty$ at $x = 0$), then its velocity grows more slowly. At long times for an infinite plane the velocity reaches a constant asymptotic velocity that depends mainly on the entrainment conditions for flows in the air:

$$U_\infty \propto \sqrt{\frac{2gh_n\left(1 + \frac{\alpha_l}{2}\right)\sin\theta\rho_s}{\alpha_v^2(1+\chi)\rho_a}}. \tag{15}$$

Because of the slow growth of the velocity, this asymptotic velocity is reached only at very long times. Without particle entrainment, the velocity reaches a maximum at approximately $x_m^2 = (2\rho_0/3\rho_a)\alpha_v^{-2}V_0/(1+\chi)$:

$$U_m^2 \approx \frac{4}{\sqrt{3}}\sqrt{\frac{\bar{\rho}_0}{\rho_a}}\frac{g\sqrt{V_0}\sin\theta}{\alpha_v\sqrt{1+\chi}},$$

then it decreases asymptotically as

$$U \propto \sqrt{\frac{8\Delta\rho_0}{3\rho_a}\frac{gV_0\sin\theta}{x}\frac{1}{\alpha_v^2(1+\chi)}}. \tag{16}$$

In this case the front position varies with time as

$$x_f \propto \left(g_0' V_0 \sin\theta\right)^{1/3} t^{2/3}. \tag{17}$$

These simple calculations show the substantial influence of the particle entrainment on cloud dynamics. In the absence of particle entrainment from the bed the fluid entrainment

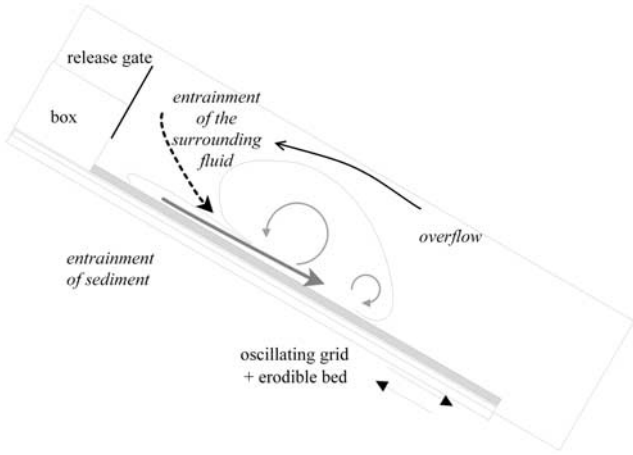

Figure 3. Sketch of the experimental setup.

has a key role since it directly affects the value of the maximum velocity that a cloud can reach.

4. Laboratory Experiments

4.1. Experimental Device, Procedure, and Qualitative Observations

[29] To supplement data obtained by *Beghin* [1979] and *Beghin et al.* [1981] for two-dimensional Boussinesq clouds without particle entrainment, Beghin ran more tests to study the influence of non-Boussinesq effects and particle entrainment. Forty-three tests were done, but a number of these were intended only to estimate variance in the data; all nonredundant data obtained by Beghin are reproduced here. We have recently made additional runs to test the sensitivity of the results to the boundary conditions (supply system and bottom roughness) [*Ancey*, 2004].

[30] The experiments were conducted using an inclined plane 2 m in length and 0.17 m in width, immersed in a closed water tank ($220\times110\times80$ cm^3). A box with a sluice gate was located at the upper part of the plane, as shown in Figure 3. It was filled with particle suspensions. The suspension volume was in the range of 1–12 L, but most runs were done with a fixed volume of 1 L; in this case the initial length l_0 was 12 cm and the initial flow depth h_0 was 5 cm, leading to an initial volume per unit width of 60 cm^2. Over the plane an oscillating grid (square grid 1×1 cm^2, 2 mm in thickness) was used to create a loose erodible bed whose particles could be entrained into the cloud. The oscillation amplitude was low (0.5 cm). Other systems (fixed grids, bentonite layer, etc.) were also tested, but none turned out to be more efficient. Without this grid, we observed that the mobile bed either was very difficult to set in motion or spontaneously slid before the cloud was released because the angle of repose of these materials fell within the range of plane inclinations (typically 30°–45°). In the absence of oscillations we observed that the material rapidly settled and was very difficult to entrain because it behaved like a cohesive-like material. Two inclinations were studied, $\theta = 30°$ and $\theta = 42°$.

[31] A compromise was necessary between how easily the sediment could be entrained into the cloud and the ability of the sediment to resist sliding down the inclined plane. This problem of selecting a suitable material was complicated by the constraints imposed by similarity conditions. For the sediment to be entrained and maintained in suspension we had to use light materials whose settling velocity was low compared to the characteristic velocity of large eddies. This can be achieved by using materials (1) whose density ρ_p does not differ substantially from the density ρ_a of the surrounding fluid or (2) whose diameter is very low. In preliminary tests made with air as the surrounding fluid we used kaolin particles. We observed a particle cloud of very high velocity followed by a rapid collapse of the cloud. The kaolin particles tended to quickly aggregate due to electrostatic effects and settled. This led us to use water as the interstitial fluid, though it made it impossible to study strongly non-Boussinesq suspensions. We used sawdust (mean typical diameter $d = 300$ or 500 μm, $\rho_p = 1170$ kg m^{-3}) as particles. Although these materials had very low settling velocities (in the range 6–8 mm s^{-1}), they also presented the disadvantage of acquiring a cohesive-like behavior when wet. With the same material, we prepared the suspension filling the box (ρ_0 in the range 1004–1100 kg m^{-3}) and the erodible bed layer (thickness in the range 0.5–2 cm and $\rho_s \approx 1085$ kg m^{-3}). Note that high concentrations of sawdust ($\varphi \approx 0.6$) must be used to obtain the heavier suspensions.

[32] Flows were filmed from the side by a camera. Images allowed us to determine the cloud dimensions and the front velocity. The height and length were estimated by adjusting a half ellipsis to the cloud. This method for measuring the cloud length seems more accurate than directly measuring the length on the pictures because the cloud was followed by a shallow tail.

[33] We observed that the particle cloud was composed of two evident eddies (see Figure 3) in agreement with *Simpson*'s [1972] observations. When the cloud moved from left to right, we observed a small vortex ahead of the front, spinning clockwise, and a large counterclockwise eddy occupying most of the cloud volume. The large eddy had a double role: It entrained not only the surrounding fluid but also the particles from the bed. Indeed, when the cloud moved over the erodible bed, particles were set in motion and formed a dense layer, whose velocity was lower than the cloud velocity. The large eddy accelerated a part of this dense layer lagging behind the cloud. In this way, particles were entrained from behind. Since experiments were done in a closed channel, as soon as the sluice gate was raised and the suspension started collapsing, a countercurrent began to flow in the opposite direction (see Figure 3). As for other lock exchange experiments [e.g., see *Simpson*, 1997], this return flow had the disturbing effect of decreasing the velocity of the cloud front by a factor 1.2–1.5, depending on the ratio of the cloud height to the channel depth. To fix this problem, we carried out more experiments in a large water tank (volume of 20 m^3 with a free surface), but we had to locate a deflector just ahead of the sluice gate to concentrate the starting flow; in the absence of this deflector on steep slopes an ill-formed cloud developed. Even with this modified experimental setup, countercurrents were observed and tended to decrease the cloud velocity.

4.2. Experimental Results and Comparison With the KSB Model Results

[34] Equations (10), (11), and (13) were solved numerically using the built-in function NDSolve included in

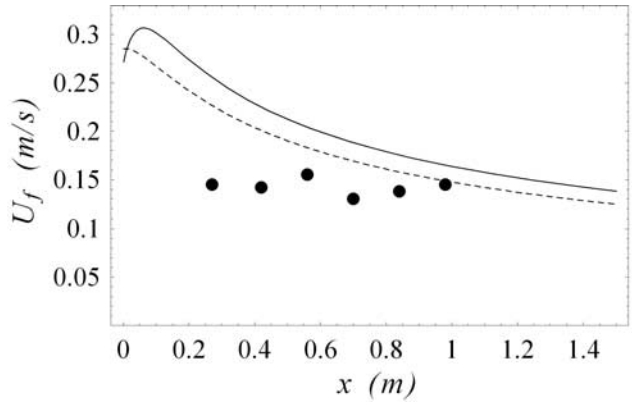

Figure 4. Velocity variation for the cloud front in a non-Boussinesq case and without particle entrainment. The experimental conditions are $\theta = 42°$, $\rho_0 = 1100$ kg m^{-3}, $\rho_a = 1000$ kg m^{-3}, $h_n = 0$ m, and $V_0 = 1$ L. Dots are the experimental data. The solid line shows simulations I (Richardson number–dependent growth rate), and the dashed line shows simulations II (bed slope-dependent growth rate).

Mathematica 4.2. As initial conditions, we took, at $x = 0$ (corresponding to the sluice gate position) $H = h_0$ (5 cm in most runs), $L = l_0$ (12 cm, in most runs), $\rho = \rho_0$ (in the range of 1004–1100 kg m^{-3}), $U = u_0 = \sqrt{2g'_0 h_0 \cos\theta}$ (dam break analogy, with $g'_0 = \Delta\ \rho_0 g/\rho_a$). The influence of the initial conditions (notably the position of the origin of the streamwise axis) was discussed by *Beghin et al.* [1981]; we simply checked that the simulations were not strongly dependent on the choice of the initial conditions (notably u_0). For the entrainment coefficient in equation (10) we examined both possibilities presented above.

[35] 1. For simulations I, the coefficients α_v, α_h, and α_l are assumed to depend on the overall Richardson number (equation (6)). They were fitted using the data from *Beghin et al.* [1981]: $\tilde{\alpha}_l = (3.75 - \mathrm{Ri})/(5.5 + 3.03\mathrm{Ri})$, $\alpha_v = (1.56 - \mathrm{Ri})/(1.16 + 1.01\ \mathrm{Ri})$, $\alpha_h = (1.53 - \mathrm{Ri})/(4.1 + 2.96\ \mathrm{Ri})/(1 - \tilde{\alpha}_l/2)$, and $\alpha_l = \tilde{\alpha}_l/(1 - \tilde{\alpha}_l/2)$.

[36] 2. For simulations II, the coefficients α_v, α_h, and α_l are assumed to depend on the bed slope θ and the density ratio $\bar{\rho}/\rho_a$. In the Boussinesq case they were obtained by *Beghin et al.* [1981] by fitting their data: $\tilde{\alpha}_l = (0.0044\theta + 0.26)$, $\alpha_v = 2\sqrt{k_v/k}\alpha_h$, $\alpha_h = (0.0036\theta + 0.04)/(1 - \tilde{\alpha}_l/2)$, and $\alpha_l = \tilde{\alpha}_l/(1 - \tilde{\alpha}_l/2)$. In the non-Boussinesq regime the coefficients above must be corrected by a multiplicative factor $\sqrt{\bar{\rho}/\rho_a}$.

[37] For the aspect ratio k, data obtained by *Beghin et al.* [1981] were used to deduce a relationship between k and θ: $k(\theta) = 0.158(1 + 0.59\theta)^{0.3}$ (θ in degrees). The front velocity was obtained by multiplying the velocity of the mass center U by $1 + \alpha_l/2$.

[38] Figure 4 provides an example of a non-Boussinesq cloud ($\Delta\rho_0/\rho_a = 0.1$) without particle entrainment on a 42° bed slope. The dots represent the measured velocities of the cloud front, the solid line corresponds to the computed velocities given by simulations I (Richardson-dependent growth rates), and the dashed line represents the result given by simulations II (slope-dependent growth rates). The two simulation curves are reasonably close (relative difference less than 25%) and show a decrease in the front velocity. If the predicted velocity magnitude is consistent with the data, there is no real decrease in the front velocity in our experiments.

[39] Figure 5 shows the velocity variation for a Boussinesq cloud ($\Delta\rho_0/\rho_a = 0.004$) with a low particle entrainment rate ($h_n = 1$ mm). As expected, the simulations show a slight increase in the front velocity, in agreement with the measurements. However, the simulations overestimate the velocity since the relative difference between the computed and the measured velocities reaches 33% for simulations II versus 80% for simulations I. Consistent with numerical simulations, a linear variation was observed in the cloud height with downstream distance (not reported here). Experimentally, we found that $\tilde{\alpha}_h = 0.16$, while simulations I provided $\tilde{\alpha}_h = 0.15$ versus 0.23 for simulations II.

[40] Figure 6 shows the velocity variation for a Boussinesq cloud in a limiting Boussinesq regime ($\Delta\rho_0/\rho_a = 0.05$) with a fairly large particle entrainment rate ($h_n = 1$ cm). A slight increase was observed experimentally in the front velocity with a maximum velocity of 14.5 cm s^{-1}, much lower than the values provided by simulations I (1.15 m s^{-1}) and simulations II (70 cm s^{-1}). In contrast, simulations I successfully provided the variations in cloud height and length. Simulations II overestimate the length and height growth rate by a factor of 2–3.

[41] Figure 7 shows the variation in the cloud velocity for a non-Boussinesq regime ($\Delta\rho_0/\rho_a = 0.1$) with particle entrainment. Both simulations predict an increase in the front velocity with the downstream distance in agreement with the measurements but grossly overestimate the velocity values by a factor of 4 for simulations I and by a factor of 2 for simulations II. Simulations I provide a fairly linear variation in cloud height with distance; nonlinear variations can be observed only in the first instants after the release. Cloud height is slightly overestimated by simulations I, by approximately 15%, but the computed growth rate, $\alpha_h = 0.15$, is consistent with the measurements. As regards cloud

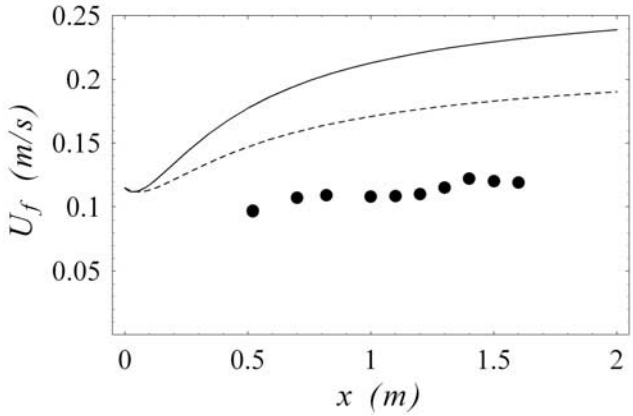

Figure 5. Velocity variation for the cloud front in the Boussinesq case. The experimental conditions are $\theta = 42°$, $\rho_0 = 1050$ kg m^{-3}, $\rho_a = 1000$ kg m^{-3}, $h_n = 1$ mm, $\rho_s = 1030$ kg m^{-3}, and $V_0 = 12$ L. Dots are the experimental data. The solid line shows simulations I (Richardson number–dependent growth rate), and the dashed line shows simulations II (bed slope-dependent growth rate).

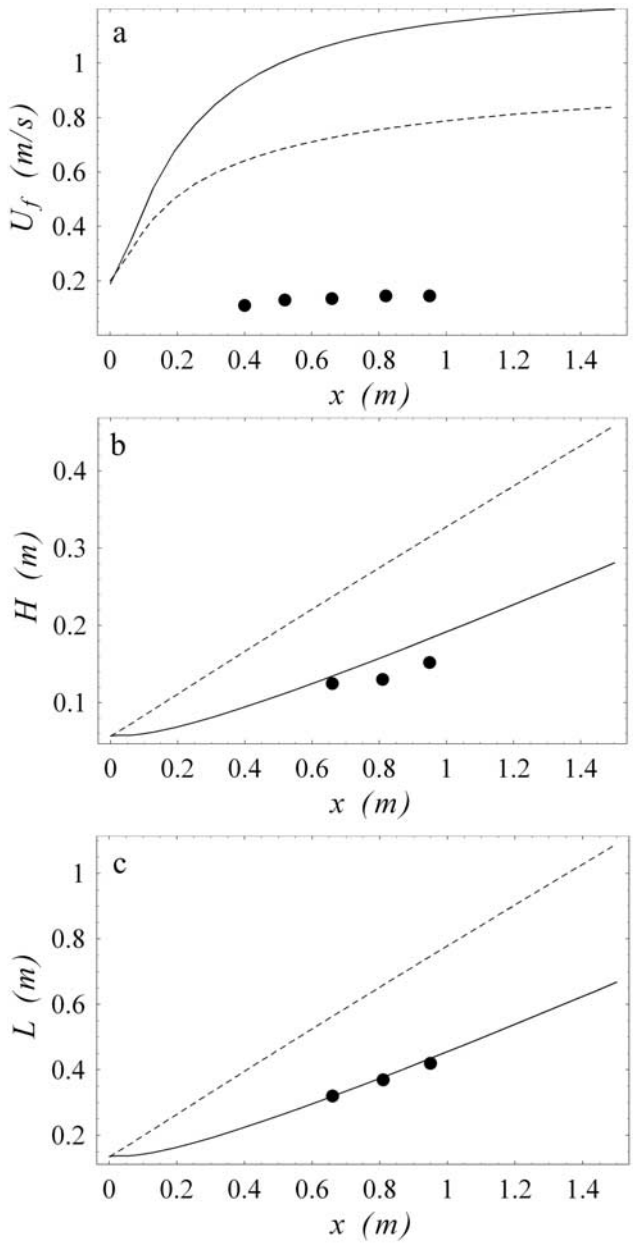

Figure 6. (a) Velocity variation for the cloud front in the non-Boussinesq case. (b) Height variations. (c) Length variations. The experimental conditions are $\theta = 42°$, $\rho_0 = 1050$ kg m^{-3}, $\rho_a = 1000$ kg m^{-3}, $h_n = 1$ cm, $\rho_s = 1085$ kg m^{-3}, and $V_0 = 1$ L. Dots are the experimental data. The solid line shows simulations I (Richardson number–dependent growth rate), and the dashed line shows simulations II (bed slope-dependent growth rate).

length, simulations I provide values in agreement with experimental data, but the experimental growth rate α_l seems somewhat larger than the computed growth rate. For both cloud height and length, simulations II provide values that are higher, by a factor of 2–3, than experimental data. Note that the data are too noisy to detect a nonlinear behavior of the curve $H(x)$.

[42] On the whole, for the different experimental conditions tested, simulations I provided good predictions of cloud height and length but significantly overestimated the front velocity. Although the relative difference between simulated and measured velocities is lower than for simulations I, simulations II yielded values in poor agreement with experimental data when flow conditions differed from the Boussinesq regime without particle entrainment. This substantial difference between measured and computed velocities in the non-Boussinesq case is surprising. Other tests made by replacing the sawdust suspension with a brine solution of the same density revealed that the velocity of a particle-driven gravity current was much lower than for a density current [*Laval et al.*, 1988]. *Hallworth and Huppert* [1998] also observed significant differences in the behavior of concentrated and dilute particle-driven gravity currents along a horizontal channel that they ascribed to an abrupt collapse of the dispersed phase: Beyond a critical initial volume concentration of particles the current came to a sudden halt, while a much thinner layer of sediment continued to extend for some distance beyond the arrest point. In the present case the large bed slope probably precluded the current from abruptly coming to rest, but the abrupt transition observed by *Hallworth and Huppert* [1998] could occur and affect the cloud velocity to a large extent.

[43] As a conclusion, from the viewpoint of laboratory experiments, neither model turns out to be completely supported by experimental data. The assumption that the growth rate α_v depends on the bed slope θ and the density ratio $\bar{\rho}/\rho_a$ receives no support in the experiments presented here. The dependence of α_v on the Richardson number Ri appears more credible, except that such an assumption leads to overestimating the cloud velocity for concentrated particle-driven gravity currents. Good results were, however, obtained for concentrated density currents.

5. Field Applications

[44] There are very few powder snow avalanche events that have been documented accurately and thoroughly. This makes it very difficult to test the efficacy of the KSB model. Here we compare the KSB model with a data series from the La Sionne site (Rhone Valley, Switzerland). The path extends on the southeast facing slope of Crêta Besse between ~2550 (2400–2700 m) and 1450 m in elevation, and its length exceeds 2.2 km. The bottom point of the path is marked by the Sionne river. Flowing avalanches can be confined in the river bed and continue to flow. On the whole, the path is open, except between 1800 and 2000 m above sea level (asl), where avalanches are confined in one or two gullies. The overall slope is high (52%); the path slope decreases rather regularly between the release zone (slope 80%) and the run-out zone (mean slope close to 30%). More information can be found in the work of *Ammann* [1999], *Dufour et al.* [2001], *Schaer and Issler* [2001], and *Vallet et al.* [2001].

[45] Here we examine only the avalanche of 25 February 1999, for which the front velocity was recorded. For two other events the variations in impact pressure with time were measured on a tubular mast and a wedge located at the elevation of 1640 m ($y \approx 1630$ m); for the avalanche of 10 February 1999 (half as large as the 25 February avalanche in terms of snow volume, $U \approx 50$ m s^{-1} and $H \approx 50$ m), *Schaer*

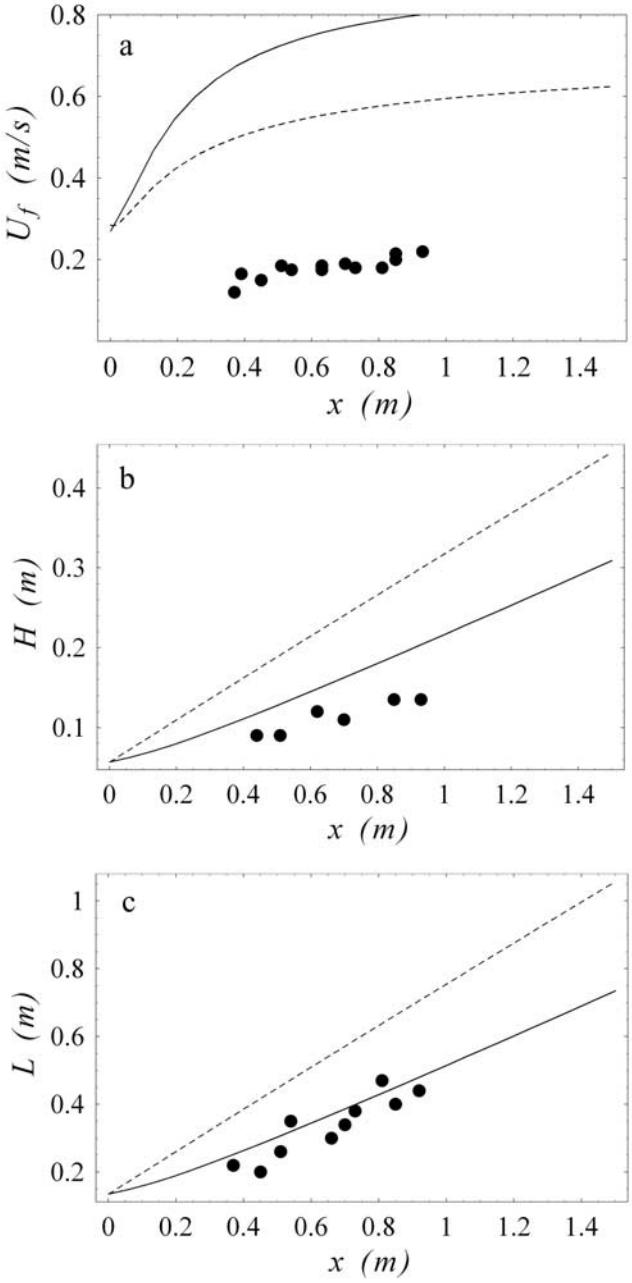

Figure 7. (a) Velocity variation for the cloud front in a limiting Boussinesq case. (b) Height variations. (c) Length variations. The experimental conditions are $\theta = 42$, $\rho_0 = 1100$ kg m^{-3}, $\rho_a = 1000$ kg m^{-3}, $h_n = 1$ cm, $\rho_s = 1085$ kg m^{-3}, and $V_0 = 1$ L. Dots are the experimental data. The solid line shows simulations I (Richardson number–dependent growth rate), and the dashed line shows simulations II (bed slope-dependent growth rate).

and Issler [2001] found that the maximum mean pressure impact was 500 kPa (with peaks exceeding 1200 kPa) at the avalanche base (3 m from the ground) but decreased rapidly with height (40–50 kPa at 7 m from the ground, 1 kPa at 19 m). There was no measurement of the flow depth, but the video films made by *Heinmann et al.* [1999] provide an estimate of the front height at the elevation of 1640 m: The front was approximately 20 m high, while the body flow depth was in the range of 40–80 m. The avalanche volume in the release zone was evaluated at 520,000 m^3, while the deposit volume was approximately 870,000 m^3. This clearly indicates that there was a significant entrainment of snow from snow cover into the avalanche.

[46] In Figure 8a we have reported the variation in the mean front velocity U_f as a function of the horizontal downstream distance y_f. The dots correspond to the measured data, while the curves represent the solution obtained by integrating equations (2)–(4) numerically and by assuming that the growth rate coefficient depends on the overall Richardson number (solid line) or the bed slope and density ratio (dashed line). For the initial conditions, on the basis of the photogrammetric study by *Vallet et al.* [2001], we assume that $u_0 = 0$, $h_0 = 2.1$ m, and $l_0 = 20$ m. It is reasonable to think that the average snow density at the snow cover surface was close to 150 kg m^{-3}; Therefore we take $\rho_0 = \rho_s = 150$ kg m^{-3}. Owing to the high path gradient between the origin and the elevation $z = 1800$ m ($y = 1250$ m), we have considered that, on average, the released snow layer h_n is 0.7 m thick and is entirely entrained into the avalanche. In simulations I the entrainment coefficient α_v was a function of the overall Richardson number Ri that was fitted on the data from *Beghin et al.* [1981]. The range of Ri values in these data is 0.23–1.32 and thus is too narrow to represent the whole range of

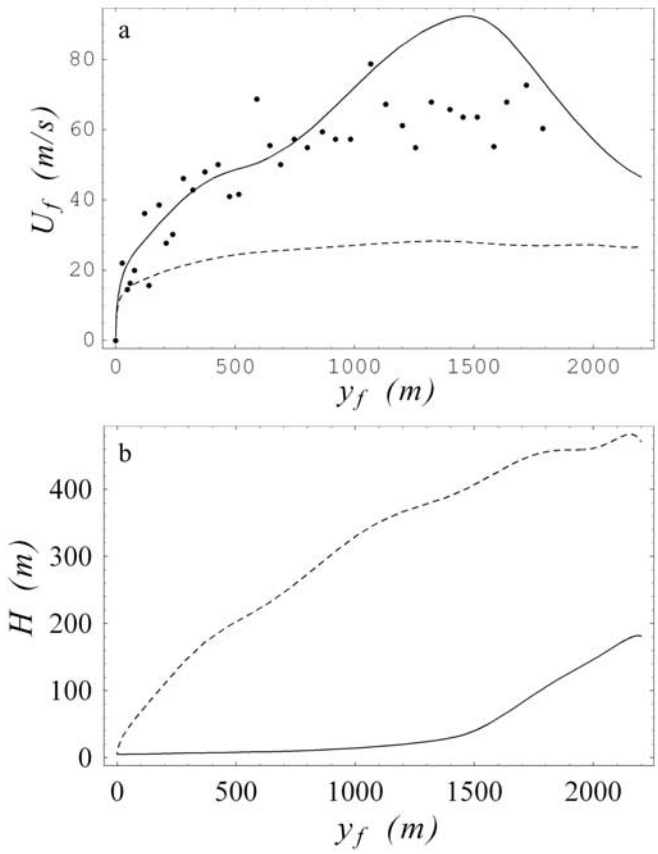

Figure 8. (a) Velocity variation for the La Sionne avalanche of 25 February 1999. (b) Cloud height. The olid line shows simulations I (Richardson number–dependent growth rate). The dashed line shows simulations II (bed slope-dependent growth rate). Dots are data from *Dufour et al.* [2001].

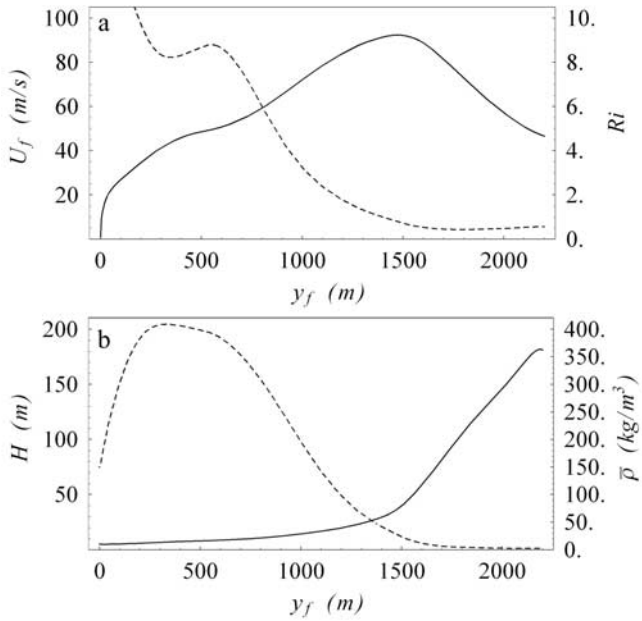

Figure 9. (a) Variation in the front velocity (solid line) and Richardson number (dashed line) with horizontal downstream distance for the La Sionne avalanche of 25 February 1999. (b) Variation in the cloud height (solid line) and mean density (dashed line).

possible values for natural events. Using $\alpha_v \propto \mathrm{Ri}^{-1}$ for $\mathrm{Ri} \gg 1$ [*Fernando*, 1991], we apply the following relationship (see Figure 2): For $\mathrm{Ri} \geq 1$, $\alpha_v = e^{-1.6\mathrm{Ri}2}$, while for $\mathrm{Ri} > 1$ we take $\alpha_v = 0.2/\mathrm{Ri}$.

[47] As shown in Figure 8a, the avalanche accelerated vigorously after the release and reached velocities as high as 80 m s^{-1}. If the entrainment rate α_v is assumed to be a function of the Richardson number (simulations I), the KSB model successfully describes the velocity variation with the downstream distance. The maximum computed velocity is 92 m s^{-1}, 13% higher than the measured value. The velocity variation in the release phase is reasonably well described by the KSB model. The model predicts a bell-shaped velocity variation, while field data provide a flatter velocity variation. The computed flow depth at z = 1640 m is approximately 60 m (see Figure 8b), which is consistent with the value estimated from the video tapes. In contrast, if the entrainment rate α_v is assumed to be a function of the local slope and the density ratio (simulations II), there is no agreement with field data: The maximum velocity is approximately 20 m s^{-1}, while the cloud height is 430 m at z = 1640 m. In line with the conclusions of the laboratory experiments, it is highly unlikely that the KSB model based on a slope-dependent growth rate can be applied to describe the non-Boussinesq regime of powder avalanches unless the entrainment coefficients are specifically fitted, depending on whether the avalanche entrains snow from the snow cover. On the contrary, expressing the growth rate as a function of only the Richardson number makes it possible to describe the velocity and height variations consistently.

[48] Figure 9 shows the variation of the front velocity U_f and the overall Richardson number Ri (Figure 9a), together with the variations in cloud height H and mean density $\bar{\rho}$. It can be seen that in the accelerating phase the Richardson number is high (typically in the range of 2–10), which limits the air entrainment into the avalanche and the cloud growth in height, consistent with field observations [*Heinmann et al.*, 1999]. Note that in the early phase the bulk density is very high (close to 400 kg m^{-3}), which suggests that in the accelerating phase a powder snow avalanche is made up of a high-density core. When the Richardson number drops under unity, there is a significant increase in the cloud height associated with a rapid cloud dilution (bulk density dropping to 10–20 kg m^{-3}). In the film made by *Heinmann et al.* [1999] a sudden rise in the cloud height can also be observed when the avalanche front descended below the elevation of 1600 m asl.

[49] In order to evaluate the sensitivity of the simulation results, we examined different values of the erodible mass. In Figure 10 we have reported the comparison between field data and computations made with three different assumptions: $\rho_s h_n$ = 50, 105, or 150 kg m^{-2}. It can be seen that there is no significant variation in the computed velocities in the accelerating phase, but both the maximum velocity and the position at which the maximum velocity is reached depend on the $\rho_s h_n$ value. By increasing the erodible mass per unit surface from 50 to 150 kg m^{-2}, the maximum velocity is increased from 69 to 105 m s^{-1}, i.e., by a factor of 1.5. Note that the dependence of the maximum velocity on the snow cover thickness is consistent with field measurements made by *Dufour et al.* [2001]: For instance, the avalanche of 10 February 1999 was approximately half as large in terms of deposited volume as the avalanche of 25 February 1999, and its maximum velocity was 25% lower than the maximum velocity recorded on 25 February 1999. This result is of great importance in engineering applications since it means that the maximum velocity and, thereby, the destructive power of a powder snow avalanche mainly result from the ability to entrain snow from the snow cover when the avalanche descends.

6. Concluding Remarks

[50] This paper has revisited the theoretical model initially proposed by *Kulikovskiy and Sveshnikova* [1977] to describe

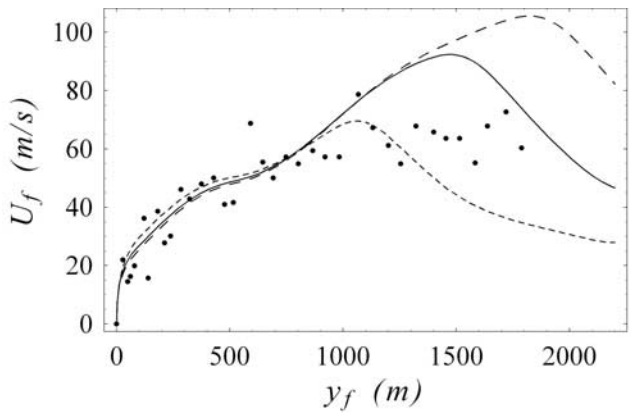

Figure 10. Dependence of the front velocity on the erodible mass. The solid line shows $\rho_s h_n$ = 105 kg m^{-2}; the dashed line shows $\rho_s h_n$ = 50 kg m^{-2}; and the long-dashed line shows $\rho_s h_n$ = 150 kg m^{-2}. Data are from *Dufour et al.* [2001].

the motion of finite-volume gravity currents in the form of a semielliptic cloud down an inclined plane. Following the simplification suggested by *Beghin* [1979], we have ignored the kinetic energy equation and only retained the volume, mass, and momentum balance equations; the model is referred to as the KSB model. The mass and volume of the cloud can vary as a result of surrounding fluid entrainment and/or particle entrainment from the bed. A central point in this model is the volume growth rate α_v resulting from the ambient fluid entrainment. Kulikovskiy and Sveshnikova suggested that this coefficient depends on the square root of the density ratio $\sqrt{\bar{\rho}/\rho_a}$, whereas Beghin considered it to be a function of the local slope θ. The slope dependence of α_v has been determined experimentally by *Beghin et al.* [1981]. Following *Ellison and Turner* [1959], this paper shows that it is possible to interpret the experimental data of *Beghin et al.* [1981] differently by assuming that the growth rate coefficient depends on the overall Richardson number Ri instead of by θ and $\sqrt{\bar{\rho}/\rho_a}$. In the Boussinesq limit and for constant slope beds the two assumptions lead to similar results, but they imply very different behaviors in the non-Boussinesq regime and/or when particles from the bed are entrained. Asymptotic solutions have been found for the accelerating phase and steady-state Boussineq regime: When the cloud accelerates after its release, the front velocity scales as $U_f \approx \sqrt{2gx\sin\theta}$, irrespective of the entrainment parameters and the initial density. This striking result seems consistent with field measurements made at the La Sionne site. When the cloud entrains particles from the bed, it reaches a limiting velocity $U_\infty = \sqrt{2gh_n \sin\theta \rho_s/(\alpha_u^2(1+\chi)\rho_a)}$, whereas if there is no particle supply, the cloud decelerates asymptotically as $U_f \propto \sqrt{g_0' V_0 \sin\theta/x}$.

[51] Experiments on the instantaneous release of finite volume, two-dimensional, heavy particle-driven gravity currents have been conducted. The currents can entrain particles from the bed, which allowed them to maintain a fairly large density difference with the ambient fluid. It is striking to note the result, probably in line with observations made by *Laval et al.* [1988] together with *Hallworth and Huppert* [1998], that concentrated particle-driven gravity currents flowed much more slowly than density currents (of the same density). When the growth rate is expressed as a Richardson number function, the KSB model provides good estimates of cloud length and height. It substantially overestimates the velocity for particle-driven gravity currents but provides good results for density currents. In contrast, the growth rate depending on θ and $\sqrt{\bar{\rho}/\rho_a}$ receives no experimental support unless the growth rate coefficients are fitted for each type of flow condition.

[52] When compared to a series of field measurements (the large powder snow avalanche of 25 February 1999 at the La Sionne site), the KSB model provides results in good agreement with the data provided: that the growth rate coefficient is expressed as a function of the Richardson number. Interestingly, the KSB model predicts front velocity more accurately for the field case than for the laboratory case. A possible explanation is related to the large difference in the viscosity and density between the air and water, implying substantial contrasts in the coupling and energy dissipation rates between the two phases. Indeed, the interplay between the fluid and solid phases is controlled by the Stokes number $\mathrm{St} \propto \rho_p a u/\mu$ (with ρ_p the particle density, a the particle radius, u the velocity of the particle relative to the fluid phase) [*Batchelor*, 1989; *Ancey et al.*, 1999]; when $\mathrm{St} \gg 1$, the particle and solid phases can be treated independently, whereas when $\mathrm{St} \to 0$, the particle phase is entirely controlled by the fluid phase. Intermediate values of the Stokes number reflect a more or less strong interplay between the two phases. In the laboratory case, replacing air with water induces a significant increase in viscosity and thus a decrease in the Stokes number, favoring a complex coupling between the two phases and high dissipation rates (due to the existence of relative velocity difference between the two phases).

[53] Compared to other powder snow avalanche models, the KSB model presented here has the advantage of relying on simple balance equations. The two parameters involved in the model, the volume growth rate coefficient $\alpha_v(\mathrm{Ri})$ and the aspect ratio $k(\theta)$, have been fitted using the *Beghin et al.* [1981] data (clouds in a Boussinesq regime); all other parameters can be deduced from these two quantities. The KSB model can be applied to a wide range of situations (with or without particle entrainment from the bed, in a Boussinesq or non-Boussinesq regime), which makes it a very attractive model. However, the discrepancy between its predictions and the laboratory experiments done with concentrated suspensions needs further investigation. Moreover, the extrapolation of $\alpha_v(\mathrm{Ri})$ to large Richardson numbers should be examined more thoroughly.

[54] The KSB model remains a simplistic approximation of real particle-driven gravity currents. It is most probably likely to provide acceptable results when the cloud is energetic enough to maintain particles in suspension. During the decelerating phase, additional effects, ignored here, must be taken into account, including particle sedimentation, density stratification, the effect of phase separation on momentum balance, the influence of the turbulent kinetic energy on bottom drag, and fluid entrainment.

Appendix A

[55] This Appendix solves the equations of motion in the Boussinesq limit. The equations of motion include the volume balance equation (10), the mass balance equation (11), and the momentum balance equation (13). Using the relation $d(\cdot)/dt = U d(\cdot)/dx$, we can write these equations:

$$\frac{dV}{dx} = \alpha_v \sqrt{V}, \tag{A1}$$

$$\frac{d\Delta\bar{\rho}V}{dx} = \rho_s \left(1 + \frac{\alpha_l}{2}\right) h_n, \tag{A2}$$

$$U \frac{d(\bar{\rho} + \chi\rho_a)VU}{dt} = \Delta\bar{\rho} g V \sin\theta, \tag{A3}$$

where the unknowns are the volume V, the velocity of the mass center U, and the bulk density $\bar{\rho}$. To simplify the analytical expressions, without loss of generality, we take, at $t = 0$ and $x_0 = 0$, $U_0 = 0$, $H = H_0$, $L = L_0$, $V_0 = k_v H_0 L_0$, and $\bar{\rho} = \bar{\rho}_0$. The shape factor k_v is given by equation (2), α_v and α_l are related together via equation (5) and are constant, and the added mass coefficient χ is given by equation (12). The remaining parameters h_n and ρ_a are assumed to be constant.

[56] The volume and density variations can be easily determined by integrating equations (A1) and (A2):

$$V(x) = \left(\sqrt{V_0} + \frac{\alpha_v}{2}x\right)^2 \tag{A4}$$

$$V(x)\Delta\bar{\rho} = \rho_s\left(1 + \frac{\alpha_l}{2}\right)h_n x + \Delta\bar{\rho}_0 V_0. \tag{A5}$$

The volume rises quadratically with the downstream distance. The buoyant density $\Delta\bar{\rho}$ first increases with the downstream distance, provided that $\Delta\bar{\rho}_s h_n > \alpha_v\ \Delta\bar{\rho}_0\sqrt{V_0}$. Then, at a critical distance $x_c - x_0 = 2\sqrt{V_0}/\alpha_v - 2V_0\Delta\bar{\rho}_0/(h_n\rho_s)$, the buoyant density starts decreasing slowly. At long times we obtain the following asymptotic variation: $\Delta\bar{\rho} \propto 4h_n\rho_s{\alpha_v}^{-2}x^{-1}$. As expected, the effect of particle entrainment is to offset the cloud dilution resulting from fluid entrainment. At short times, particle entrainment is the prevailing mechanism leading to an increase in the buoyant density. At long times, despite particle entrainment, the cloud dilutes but particle entrainment still plays a role by controlling the decrease rate. Without particle entrainment, the cloud dilutes more quickly: $\Delta\bar{\rho} \propto 4\ V_0\ \rho_0{\alpha_v}^{-2}x^{-2}$ instead of $\Delta\bar{\rho} \propto x^{-1}$. The cloud dimensions can be easily deduced from equation (A4). For instance, the cloud height is

$$H(x) = \sqrt{\frac{k}{k_v}V(x)} = \sqrt{\frac{k}{k_v}}\left(\sqrt{V_0} + \frac{\alpha_v}{2}x\right) \propto \alpha_h x,$$

which is consistent with the result obtained by directly integrating equation (3).

[57] Using equations (A4) and (A5) in the momentum balance equation (A3), we obtain

$$U\frac{d}{dt}\left(A + Bx + Cx^2\right)U = D + Ex,$$

with

$$A = (\Delta\bar{\rho}_0 + (1+\chi)\rho_a)V_0, \tag{A6}$$

$$B = \rho_s\left(1 + \frac{\alpha_l}{2}\right)h_n + (1+\chi)\rho_a\sqrt{V_0}\alpha_v, \tag{A7}$$

$$C = (1+\chi)\rho_a\frac{\alpha_v^2}{4}, \tag{A8}$$

$$D = \Delta\bar{\rho}_0 V_0 g\sin\theta, \tag{A9}$$

$$E = \rho_s\left(1 + \frac{\alpha_l}{2}\right)g h_n \sin\ \theta. \tag{A10}$$

The solutions to equation (A3) can be found after algebraic manipulations. The single positive solution is

$$U(x) = \frac{\sqrt{2ADx + (BD + AE)x^2 + \frac{2}{3}(CD + BE)x^3 + \frac{1}{2}CEx^4}}{A + Bx + Cx^2}. \tag{A11}$$

Note that without entrainment from the bed ($E = 0$), the velocity varies asymptotically as

$$U(x) \propto \sqrt{\frac{2D}{3C}}\frac{1}{\sqrt{x}} = \sqrt{\frac{8}{3}\frac{\Delta\bar{\rho}_0}{\rho_a}\frac{1}{(1+\chi)\alpha_v^2}}\sqrt{\frac{gV_0\sin\theta}{x}}.$$

When the cloud entrains particles from the bed ($E > 0$), the velocity reaches an asymptotic value

$$U_\infty \propto \sqrt{\frac{2gh_n\left(1 + \frac{\alpha_l}{2}\right)\sin\theta\rho_s}{\alpha_v^2(1+\chi)\rho_a}}.$$

In both cases, this entails that the Richardson number of equation (6) tends toward a constant value:

$$\mathrm{Ri}_n(\theta) = n\frac{\cos\theta}{\sin\theta}(1+\chi)\alpha_h,$$

with $n = 3/2$ if there is no particle entrainment from the bed and $n = 8$ in the converse case. This justifies the assumption used above; that is, the growth rate coefficients are constant for a given slope. Indeed, in the Boussinesq regime, $\bar{\rho} \approx \rho_a$ and $\mathrm{Ri} \approx \mathrm{Ri}_n(\theta)$ so that whatever the expression chosen for α_v in the volume balance equation (10), its value is constant.

[58] **Acknowledgments.** I thank Margarita Eglit for providing a number of papers written by Russian scientists and for her careful reading of this paper. I thank Daniel Lhuillier for helpful references and K. Hutter for his review. Specific thanks to François Dufour, who kindly received us at his site, and to the Federal Institute for Snow and Avalanche Research (Davos, Switzerland), which provided the field data. This work is dedicated to the memory of my colleagues Philippe Revol and Pierre Beghin. I also thank Marie Clément, Frédéric Ousset, Christian Edmond-Gris, and Rémi Magnard, who helped me in conducting further experiments in the Cemagref laboratory. I am grateful to the Institut National of Sciences de l'Univers of the CNRS (grant PNRN 00CV093) for financial support through the Programme National sur les Risques Naturels.

References

Akiyama, J., and M. Ura (1999), Motion of 2D buoyant clouds downslope, *J. Hydraul. Eng.*, *125*, 474–480.

Ammann, W. J. (1999), A new Swiss test-site for avalanche experiments in the Vallée de la Sionne, *Cold Region Sci. Technol.*, *30*, 3–11.

Ammann, W., (Ed.) (2000), *Der Lawinenwinter 1999*, Schnee und Lawinen Forsch., Davos, Switzerland.

Ancey, C. (2001), Snow avalanches, in *Geomorphological Fluid Mechanics: Selected Topics in Geological and Geomorphological Fluid Mechanics*, *Lecture Notes Phys.*, vol. 582, edited by N. J. Balmforth and A. Provenzale, pp. 319–338, Springer-Verlag, New York.

Ancey, C. (2004), Influence of particle entrainment from bed on the power-avalanche dynamics, *For. Snow Landscape*, in press.

Ancey, C., P. Coussot, and P. Evesquem (1999), A theoretical framework for very concentrated granular suspensions in a steady simple shear flow, *J. Rheol. N. Y.*, *73*, 1673–1699.

Baines, P. G. (2001), Mixing in flows down gentle slopes into stratified environments, *J. Fluid Mech.*, *443*, 237–270.

Batchelor, G. K. (1967), An Introduction to Fluid Dynamics, *Cambridge Univ. Press, New York*.

Batchelor, G. K. (1989), A brief guide to two-phase flow, in *Theoretical and Applied Mechanics*, edited by P. Germain, J. M. Piau, D. Provenzale, pp. 27–41, Elsevier Sci., New York.

Beghin, P. (1979), Etude des bouffées bidimensionnelles de densité en écoulement sur pente avec application aux avalanches de neige poudreuse, Ph.D. thesis, Inst. Nat. Polytech. de Grenoble, France.

Beghin, P., and G. Brugnot (1983), Contribution of theoretical and experimental results to powder-snow avalanche dynamics, *Cold Region Sci. Technol.*, *8*, 63–73.

Beghin, P., and X. Olagne (1991), Experimental and theoretical study of the dynamics of powder snow avalanches, *Cold Region Sci. Technol.*, *19*, 317–326.

Beghin, P., E. J. Hopfinger, and R. E. Britter (1981), Gravitational convection from instantaneous sources on inclined boundaries, *J. Fluid Mech.*, *107*, 407–422.

Bozhinskiy, N., and K. S. Losev (1998), *The Fundamentals of Avalanche Science*, translated from Russian by C. E. Bartelt, *Commun.*, *55*, Schnee und Lawinen Forsch., Davos, Switzerland.

Britter, R. E., and P. F. Linden (1980), The motion of the front of a gravity current travelling down an incline, *J. Fluid Mech.*, *99*, 531–543.

Capart, H., and D. L. Young (1998), Formation of a jump by the dam-break wave over a granular bed, *J. Fluid Mech.*, *372*, 121–135.

Dufour, F., U. Gruber, and W. J. Ammann (2001), Sur la piste des avalanches catastrophes, *Les Alpes*, *2*, 9–15.

Eglit, M. E. (1983), Some mathematical models of snow avalanches, in *Advances in the Mechanics and the Flow of Granular Materials*, edited by M. Shahinpoor, pp. 577–588, Trans. Tech. Publ., Clausthal-Zellerfeld, Germany.

Eglit, M. E. (1984), Theoretical approaches to avalanche dynamics, in *Soviet Avalanche Research and Avalanche Bibliography Update: 1977–1983*, pp. 63–117, *Glaciol. Data Rep. GD-16*, U.S. Dep. of Agric. For. Serv., Washington, D.C.

Eglit, M. E. (1998), hematical and physical modelling of powder-snow avalanches in Russia, *Ann. Glaciol.*, *26*, 281–284.

Eglit, M. E., and P. Revol (1998), Models for powder snow avalanches: Comparison of two approaches, in *25 Years of Snow Avalanche Research*, edited by E. Hestnes, pp. 99–103, Norw. Geotech. Inst., Voss, Norway.

Ellison, T. H., and J. S. Turner (1959), Turbulent entrainment in stratified flows, *J. Fluid Mech.*, *6*, 423–448.

Fernando, H. J. S. (1991), Turbulent mixing in stratified fluids, *Annu. Rev. Fluid Mech.*, *23*, 455–493.

Fraccarollo, L., and H. Capart (2002), Riemann wave description of erosional dam break flows, *J. Fluid Mech.*, *461*, 183–228.

Fukushima, Y., and G. Parker (1990), Numerical simulation of powder-snow avalanches, *J. Glaciol.*, *36*, 229–237.

Fukushima, Y., T. Hagihara, and M. Sakamoto (2000), Dynamics of inclined suspension thermals, *Fluid Dyn. Res.*, *26*, 337–354.

Hallworth, M. A., and H. E. Huppert (1998), Abrupt transitions in high-concentrations, particle-driven gravity currents, *Phys. Fluids*, *10*, 1083–1087.

Heinmann, M., U. Gruber, and A. Roth (1999), *Video Films of the Sionne Avalanches of 30 January, 10, and 25 February 1999*, Schnee und Lawinen Forsch., Davos, Switzerland.

Hogg, A. H., and A. W. Woods (2001), The transition from inertia- to bottom-drag-dominated motion of turbulent gravity current, *J. Fluid Mech.*, *449*, 201–224.

Hopfinger, E. J., and J.-C. Tochon-Danguy (1977), A model study of powder-snow avalanches, *J. Glaciol.*, *81*, 343–356.

Hutter, K. (1996), Avalanche dynamics, in *Hydrology of Disasters*, edited by V. P. Singh, pp. 317–392, Kluwer Acad., Norwell, Mass.

Issler, D. (1998), Modelling of snow entrainment and deposition in powder-snow avalanches, *Ann. Glaciol.*, *26*, 253–258.

Kulikovskiy, A. G., and E. I. Sveshnikova (1977), A model for computing powdered snow avalanche motion (in Russian), *Data Glaciol. Stud.*, *31*, 74–80.

Laval, A., M. Cremer, P. Beghin, and C. Ravenne (1988), Density surges: Two-dimensional experiments, *Sedimentology*, *35*, 73–84.

Lhuillier, D. (1982), On the equation of motion of a rigid sphere in a non-uniform and accelerated inviscid fluid: Incidence on two-phase flow equations, *Mech. Res. Comm.*, *9*, 295–299.

Linden, P. F. (2000), Convection in the environment, in *Perspectives in Fluid Dynamics*, edited by G. K. Batchelor, H. K. Moffatt, and M. G. Worster, pp. 289–346, Cambridge Univ. Press, New York.

McClung, D. M., and P. A. Schaerer (1993), *The Avalanche Handbook*, Mountaineers, Seattle, Wash.

Naaim, M., and I. Gurer (1997), Two-phase numerical model of powder avalanche: Theory and application, *J. Nat. Hazard*, *16*, 18–145.

Nazarov, A. N. (1991), Mathematical modelling of a snow-powder avalanche in the framework of the equations of two-layer shallow water, *Fluid Dyn.*, *12*, 70–75.

Nishimura, K., F. Sandersen, K. Kristensen, and K. Lied (1995), Measurement of powder snow avalanche—Nature, *Surv. Geophys.*, *16*, 649–660.

Parker, G., Y. Fukushima, and H. M. Pantin (1986), Self-accelerating turbidity currents, *J. Fluid Mech.*, *171*, 145–181.

Pawlak, G., and L. Armi (1998), Vortex dynamics in a spatially accelerating shear layer, *J. Fluid Mech.*, *376*, 1–35.

Pritchard, D., and A. J. Hogg (2002), On sediment transport under dam-break flow, *J. Fluid Mech.*, *473*, 265–274.

Rooney, G. G., and P. F. Linden (1996), Similarity considerations for non–Boussinesq plumes in an unstratified environment, *J. Fluid Mech.*, *318*, 237–250.

Sampl, P. (1993), Current status of the AVL avalanche simulation model—Numerical simulation of dry snow avalanches, in *International Workshop on Gravitational Mass Movements*, edited by L. Buisson and G. Brugnot, pp. 269–278, Cemagref Editions, Antony, France.

Schaer, M., and D. Issler (2001), Particle densities, velocities and size distribution in large avalanches from impact-sensor measurements, *Ann. Glaciol.*, *32*, 321–328.

Scheiwiller, T., K. Hutter, and F. Hermann (1987), Dynamics of powder snow avalanches, *Ann. Geophys., Ser. B*, *5*, 569–588.

Simpson, J. E. (1972), Effects of a lower boundary on the head of a gravity current, *J. Fluid Mech.*, *53*, 759–768.

Simpson, J. E. (1997), *Gravity Currents in the Environment and the Laboratory*, Cambridge Univ. Press, New York.

Stacey, M. W., and A. J. Bowen (1988), The vertical structure of density and turbidity currents: Theory and observations, *J. Geophys. Res.*, *93*, 3528–3542.

Strang, E. J., and H. J. S. Fernando (2001), Entrainment and mixing in stratified shear flows, *J. Fluid Mech.*, *428*, 349–386.

Turner, J. S. (1973), *Buoyancy Effects in Fluids*, Cambridge Univ. Press, New York.

Turner, J. S. (1986), Turbulent entrainment: The development of the entrainment assumption, and its application to geophysical flows, *J. Fluid Mech.*, *173*, 431–471.

Vallet, J., U. Gruber, and F. Dufour (2001), Photogrammetric avalanche volume measurements at Vallée de la Sionne, Switerland, *Ann. Glaciol.*, *32*, 141–146.

Woods, A. W. (1997), A note on non-Boussinesq plumes in an incompressible stratified environment, *J. Fluid Mech.*, *345*, 347–356.

C. Ancey, Environmental Hydraulics Laboratory, Swiss Federal Institute of Technology, CH-1015 Lausanne, Switzerland. (christophe.ancey@epfl.ch)